

Effects of nitrogen substitution in amorphous carbon films on electronic structure and surface reactivity studied with x-ray and ultra-violet photoelectron spectroscopies




著者 (英)	Yuma Murata, Rempei Nakayama, Fumihiko Ichihara, Hiroshi Ono, Cheow-Keong Choo, Katsumi Tanaka
journal or publication title	Journal of Applied Physics
volume	121
number	9
page range	095302
year	2017-03-01
URL	http://id.nii.ac.jp/1438/00008844/

doi: 10.1063/1.4976810

Effects of nitrogen substitution in amorphous carbon films on electronic structure and surface reactivity studied with x-ray and ultra-violet photoelectron spectroscopies

Cite as: J. Appl. Phys. **121**, 095302 (2017); <https://doi.org/10.1063/1.4976810>

Submitted: 31 August 2016 . Accepted: 05 February 2017 . Published Online: 01 March 2017

Yuma Murata , Rempei Nakayama, Fumihiko Ichihara, Hiroshi Ono, Cheow-Keong Choo , and Katsumi Tanaka 



View Online



Export Citation



CrossMark

ARTICLES YOU MAY BE INTERESTED IN

[Electron transport in Al-Cu co-doped ZnO thin films](#)

Journal of Applied Physics **121**, 095303 (2017); <https://doi.org/10.1063/1.4977470>

[Surface intermixing by atomic scale roughening in Sb-terminated InAs](#)

Journal of Applied Physics **121**, 095301 (2017); <https://doi.org/10.1063/1.4976682>

[Characterization of iron doped indium phosphide as a current blocking layer in buried heterostructure quantum cascade lasers](#)

Journal of Applied Physics **121**, 094502 (2017); <https://doi.org/10.1063/1.4977243>

Ultra High Performance SDD Detectors



See all our XRF Solutions

Effects of nitrogen substitution in amorphous carbon films on electronic structure and surface reactivity studied with x-ray and ultra-violet photoelectron spectroscopies

Yuma Murata,^{1,a)} Rempei Nakayama,¹ Fumihiko Ichihara,^{1,b)} Hiroshi Ono,¹ Cheow-Keong Choo,² and Katsumi Tanaka^{1,c)}

¹Graduate School of Informatics and Engineering, The University of Electro-Communications, 1-5-1 Chofugaoka, Chofu, Tokyo 182-8585, Japan

²Center for International Programs and Exchange, The University of Electro-Communications, 1-5-1 Chofugaoka, Chofu, Tokyo 182-8585, Japan

(Received 31 August 2016; accepted 5 February 2017; published online 1 March 2017)

We investigated the effects of incorporating a low percentage of nitrogen on the local and the electronic structures of amorphous carbon (a-C) using X-ray photoelectron spectroscopy and ultra-violet photoelectron spectroscopy (UPS). Nitrogen-doped amorphous carbon films (a-CN_x) with varying nitrogen contents were prepared by a thermal decomposition method using a mixture of CH₄ + NH₃ under atmosphere. A slight shift of the C 1s core-level spectrum toward the higher binding energy side was detected in a-CN_x as a function of nitrogen content, whereas a shift of the Fermi level (E_F) cannot be confirmed from the UPS results. This was interpreted as a chemical shift between carbon and nitrogen atoms rather than as a shift of the E_F . The C 1s peak shifts can be explained by the presence of two kinds of C–N local structures and the charge transferred bulk C–C components by nitrogen atoms. The two kinds of deconvoluted C 1s components could be well correlated with the two N 1s components. Two localized states were detected below the E_F in UPS spectra of a-CN_x, which could be assigned to defect bands. These defects played a significant role in the surface reactivity, and were stabilized in a-CN_x. The adsorption and reaction of NO were carried out on a-CN_x as well as a-C films. It was found that both defect sites and O²⁻ species were responsible on a-C, while O²⁻ species were selectively active for NO adsorption on a-CN_x. We concluded that nitrogen doping reduces defect density to stabilize the surface of a-C, while at the same time inducing the selective adsorption capability of NO. *Published by AIP Publishing.*
<http://dx.doi.org/10.1063/1.4976810>

I. INTRODUCTION

Amorphous carbon (a-C) coating with high hardness, referred to as diamond-like carbon (DLC), is widely used in various industrial fields as an environmentally benign coating material in place of Cr³⁺. This coating has advantageous properties, such as high mechanical hardness, low friction, chemical inertness, and optical transparency.^{1–5} In general, a-C film consists of hybridized sp³ and sp² carbons, and hydrogen atoms in hydrogenated cases. In addition to its use as a coating material, a-C has been considered an attractive semiconductor material, because its physical properties strongly depend on the hybridized C ratio (sp³C/sp²C), C–H configuration, and atomic H content.⁵ For instance, the electronic properties and band gap values can be controlled by impurity doping. Over the past few decades, there have been many efforts to dope a-C with N, B, and P atoms.^{6–9} Especially, interesting investigations have examined the influence of nitrogen doping on a-C's electronic properties

and semiconductor characteristics, as well as the host amorphous structure.^{8,10–14}

Furthermore, because of the predication of extremely hard β-C₃N₄,¹⁵ the synthesis of amorphous carbon nitride (a-CN_x) thin films containing as high a nitrogen content as possible has been of considerable interest.^{16–18} These a-CN_x films have been extensively studied for application to semiconductor devices, as well as for wear protection.^{19,20} In recent years, nitrogen-doped carbon-based materials, such as two-dimensional (2D) N-doped graphene,²¹ one-dimensional (1D) N-doped carbon nanotube (N-doped CNT),²² graphitic C₃N₄ (g-C₃N₄),^{23,24} and the nitrogen-vacancy (NV) center of diamond,²⁵ have attracted great interest from both scientific and technological points of view, based on the idea of applying carbon allotropes to future electronic devices. Therefore, it is necessary that we gain an understanding of the nature of the chemical bond relationship between nitrogen and carbon atoms in a-CN_x.

Amorphous CN_x thin films have been prepared by various techniques, such as plasma-enhanced chemical vapor deposition, sputtering, and pulsed laser ablation.²⁶ To achieve the synthesis of a-CN_x with higher nitrogen content (~20 at. %), physical vapor deposition techniques have been generally used.^{27–29} In case of the nitrogen doping into sp³-dominant tetrahedral a-C (ta-C), the electrical resistance

^{a)}Electronic mail: murata@mail.uec.jp

^{b)}Present addresses: Graduate School of Chemical Sciences and Engineering, Hokkaido University, Sapporo 060-8628, Japan and Photocatalytic Materials Group, National Institute for Materials Science (NIMS), 1-1 Namiki, Tsukuba, Ibaraki 305-0044, Japan.

^{c)}Author to whom correspondence should be addressed. Electronic mail: katanaka@ee.uec.ac.jp

reduces due to a preferential formation of the N bonds to sp^2 carbon atoms, and only a few studies show that nitrogen doping into a-C leads to an increase of resistance.^{8,14,30,31} Most of a-CN_x thin films prepared by conventional methods show some semiconductor properties.^{32–34} It is thus expected that the physical properties of amorphous carbon films should depend on nitrogen content, as well as deposition methods. Therefore, (a) how nitrogen atoms are involved in the amorphous carbon network, (b) either they are bonded to sp^2 C or sp^3 C configuration of carbon atoms, and (c) whether or not the doping behavior of nitrogen atoms to a-C depend on deposition methods, are quite interesting subjects to study.

The effects of incorporating nitrogen on the bulk and the electronic structure, as well as on the electrical properties of a-C, has been studied but not fully elucidated. We will briefly summarize the sizeable amount of characterization data of a-CN_x, studied by X-ray photoelectron spectroscopy (XPS), ultra-violet photoelectron spectroscopy (UPS), and Raman spectroscopy.^{8,10,35} First, slight nitrogen-doping leads to a shift of the Fermi level (E_F) towards the bottom of the conduction band as an n-type dopant. Second, with higher nitrogen content, structural changes are induced in the form of an extension of band tails. In the present work, we report that a low percentage of nitrogen atoms distributed into a-C strongly affects the charge densities on bulk C-C bonds. Such an effect on the local density of state (DOS) of C-C implies a delocalization of the three-dimensional (3D) phase change of a-CN_x, which can be compared with the localization effect of a nitrogen atom in the 2D phase of N-doped graphene.^{36–38}

Since the a-C structure is unknown (amorphous) with a random network, atomic-scale local structures, such as defects, should be present both in the bulk and on the surface, and they might almost be responsible for the physical and chemical properties.³⁹ Scanning tunneling microscopy (STM) with scanning tunneling spectroscopy (STS) is one of the most powerful tools for detecting atomic-scale local structures. Recently, the local structures of nitrogen and the defect site in N-doped graphene have been revealed by combined STM/STS studies.^{36–38} However, the direct observation of local structures with STM/STS is limited to well-defined crystal surfaces, whereas it is quite difficult to detect defect sites on the chaotic surface of amorphous materials. In this study, nitric oxide (NO) was used as a molecular probe to characterize the chemical properties and local structure on the a-C surface. The electronic configuration of molecular orbitals of NO is as follows: $(4\sigma)^2 (1\pi)^4 (5\sigma)^2 (2\pi^*)^1$. An NO molecule can either donate an electron to the surface to be adsorbed as an NO⁺ species (NO⁺(a)), or accept an electron from the surface to be adsorbed as an NO⁻ species (NO⁻(a)).⁴⁰ This is because it possesses an unpaired electron in the anti-bonding $2\pi^*$ orbital. The adsorption behavior of NO is so unique that NO adsorption experiments have been carried out on a-C/a-CN_x thin films to interpret the chemical properties on the surfaces and the nature of adsorption sites from a donor-acceptor electronic point of view. They can be compared with CO, which can act as an electron acceptor because it has an empty $2\pi^*$ orbital.

In this paper, we investigated the effects of a low percentage of nitrogen-incorporation on the local and the electronic structures of a-C with XPS/UPS combined analyses in order to understand the role of nitrogen atoms in a-CN_x. In addition, we investigate the local structure and chemical properties of the a-C and a-CN_x surfaces by NO adsorption and the reaction with NO.

II. EXPERIMENTAL

Both a-CN_x and non-doped a-C thin films were deposited on ceramic (99.5% Al₂O₃) substrates by the pyrolysis reaction with a mixture of CH₄ + Ar (1:9) gas with/without NH₃ at atmospheric pressure. Our previous study contains a schematic diagram of the hydrocarbons pyrolysis method.^{41–43} Before receiving deposits, ceramic substrates were cleaned in ethanol and acetone with an ultrasonic cleaner. The substrate was then placed in the center of a ceramic tube, and a mixed gas of CH₄ + Ar and NH₃ was introduced into the tube, with a NH₃/CH₄ ratio of 0, 0.1, 0.2, 0.4, and 2.0. The ceramic tube was heated up to the setting temperature of 1373 K for 2 h with a furnace, and that temperature was maintained for 2 h. After the deposition reaction, the reactant gas was replaced with Ar, and the furnace temperature was cooled down to room temperature (r.t.). The prepared thin films were exposed to air and then transferred to XPS/UPS system.

All XPS/UPS experiments were carried out at r.t. with a VG Scientific ESCALAB MK II spectrometer at a base pressure below 1×10^{-9} Torr range. Core-level photoemission spectra were recorded at a pass energy of 20 eV using non-monochromatic Al *K* α ($h\nu = 1486.6$ eV) radiation. The overall energy resolution, including the x-ray source and analyzer, was about 1.0 eV at the full-width at half maximum (FWHM). The binding energy (BE) scale was calibrated by the Au 4f_{7/2} core-level peak at 84.0 eV. The core-level BE shifts were determined within the ± 0.1 eV accuracy. The thickness and conductivity of the films were in the order of μm and $\sim 10^4$ (S/m).⁴¹ The charging effect could be avoided because of the sufficient thickness and high conductivity even on ceramic substrate. In addition, carbon films can be deposited on ceramic substrate all over the front, rear, and side surfaces.

The obtained C 1s, N 1s, and O 1s core-level spectra were analyzed using a mix of Gaussian and Lorentzian fitting with a Shirley-type background. UPS spectra were recorded at a pass energy of 1.0 eV using He I ($h\nu = 21.2$ eV) with an energy resolution of 0.1 eV. The E_F was referenced to the Fermi edge of Au.

Before the NO adsorption experiment, samples were heated at 873 K in the preparation chamber at a base pressure below 1×10^{-9} Torr range in order to remove surface contamination. The sample temperature was monitored with a chromel-alumel thermocouple. The film surface was exposed to a 3600 L (1 Langmuir; 1 L = 1×10^{-6} Torr s) of NO gas at r.t. through a UHV metal leak valve in a preparation chamber. After the NO exposure at 3600 L, samples were transferred to the analysis chamber, and the XPS/UPS measurements were carried out at r.t.

III. RESULTS AND DISCUSSION

A. Film compositions

Nitrogen content x in the N-doped a-C films (x values of CN_x) were measured quantitatively by the integral intensity ratios (N/C) of N 1s to C 1s core-level XPS spectra after considering their atomic sensitivity factors. The nitrogen contents are plotted as a function of ammonia fraction in methane (NH_3/CH_4) in Fig. 1. The values were 0, 0.027, 0.034, 0.04, and 0.04 at the NH_3/CH_4 ratios of 0, 0.1, 0.2, 0.4, and 2.0, respectively. The x value in the CN_x film was gradually increased to 0.04 up to the NH_3/CH_4 ratio of 0.4, and was constant up to the ratio of 2.0. It was noted that the nitrogen content was uniformly constant all over the surface of the a- CN_x prepared by our method. Such limited N content has commonly been found in several studies of CN_x synthesis focused on achieving high N content to prepare crystalline C_3N_4 .²⁹ Thermal chemical vapor deposition under atmosphere has been used to understand the basic structural stability of nitrogen substitution for carbon, as well as the controllable N-doping mechanism.

In previous research, we confirmed that the films are also homogeneous on the depth scale by XPS depth profiling with Ar^+ sputtering.⁴¹ It is considered that nitrogen atoms should be homogeneously dispersed and replaced with some carbon atoms without the formation of a nitrogen-rich area in the films because of the thermal equilibrium between nitrogen and carbon atoms during thermal decomposition of ammonia and methane, as well as the deposition process of decomposed species. This was responsible for the structural stability of CN_x films prepared by our procedure.

B. XPS C 1s and N 1s core-level spectra

Fig. 2 shows the C 1s and N 1s core-level spectra for a- CN_x films with x values of nitrogen content ($x = 0, 0.027, 0.034, 0.04$), as shown in Fig. 1. As the nitrogen content increased from 0 to 0.04, the C 1s core-level spectra demonstrated a gradual shift towards the higher BE side with an asymmetric broadening. The peak BE value and the FWHM of C 1s spectra are plotted as a function of the x value in the CN_x film in Fig. 3. The N 1s spectra consist of the two major components located at 398.5 eV (FWHM: ~ 2.0 eV) and 401.4 eV (FWHM: ~ 2.0 eV). Many XPS studies on a- CN_x have attempted to characterize the role of the C-N chemical bond on bulk properties such as smoothness.^{28,44–48} However, the nature of the C-N bond remains unclear

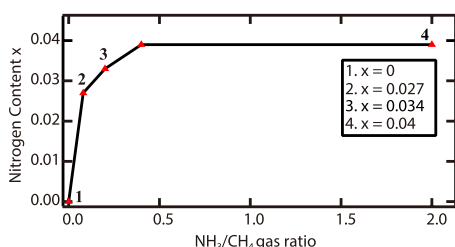


FIG. 1. Nitrogen content x of a- CN_x ($x = 0, 0.027, 0.034, \text{ and } 0.04$) as a function of NH_3/CH_4 gas ratio. In this study, the samples labeled 1, 2, 3, and 4 were characterized with XPS/UPS.

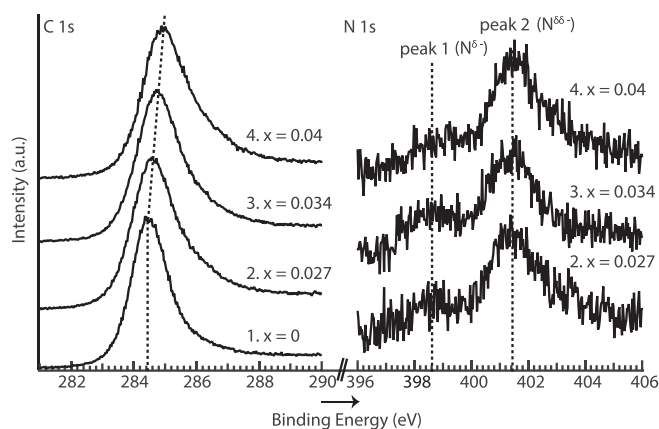


FIG. 2. C 1s (left) and N 1s (right) core-level spectra based on nitrogen content x ($x = 0, 0.027, 0.034, 0.04$). The dashed line in C 1s shows the change of BE position based on nitrogen content. Peak 1 (~ 398.5 eV) and peak 2 (~ 401.4 eV) of N 1s core-level are denoted as $\text{N}^{\delta-}$ and $\text{N}^{\delta+}$, respectively.

because a variety of nitrogen configurations with an unresolved chemical shift are present. In the N 1s peak assignment for a- CN_x , N 1s peaks with lower BE (398–399 eV) and higher BE (400–402 eV) are generally assigned to N atoms with sp^3 -coordinated C atoms (N- sp^3C) and sp^2 -coordinated C atoms (N- sp^2C), respectively.^{28,44–47} On the other hand, for N-doped graphene, which is connected with a 2D network of sp^2 hybridized carbon atoms, these peaks have been referred to as pyridine-like C–N (398–399 eV) and graphite-like C–N (400–402 eV), respectively.^{49,50} The N 1s BE values remain constant with the increase of nitrogen content. Only the minor shift of C 1s towards the higher BE side can be interpreted as a charge transfer from C (electronegativity (EN): 2.5 (Ref. 51)) to N (EN: 3.0 (Ref. 51)).

It has been reported that the electron density of the C atoms decreases depending on the different electronegativities, and as a result induces a shift of the C 1s core-level line towards the higher BE side.³⁵ Even a moderate polarization of carbon bonds leads to a significant BE shift, for instance,

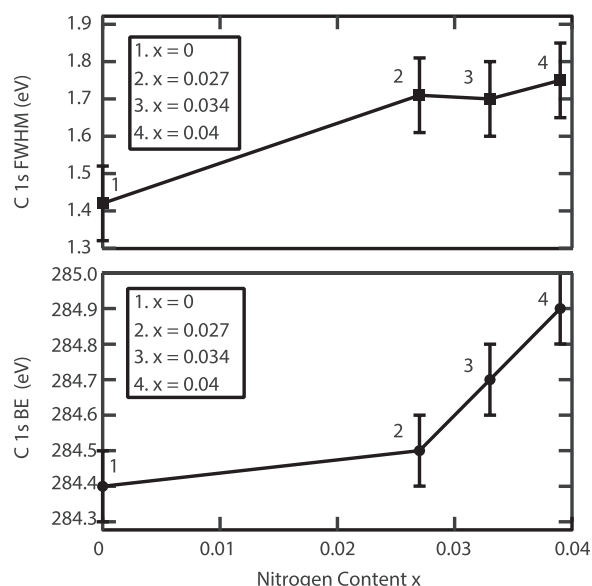


FIG. 3. C 1s BE position and FWHM as a function of nitrogen content x .

pyridine (285.5 eV) and hexamethylene-tetramine (286.9 eV).²⁸ Here, let us consider the reason why incorporation of even a low percentage of N into the host carbon material (a-C) affects the C 1s main peak position shift. Based on a simple interpretation of the XPS chemical shift, only the C–N component seems to be a candidate as the species was detected at the higher BE side of the C 1s spectra. As for N-doped graphene, only the C–N component located at around 285.5 eV in the C 1s core level is found without inducing a shift of the C 1s main peak even at high nitrogen content (~ 16 at. %).⁵² On the other hand, an upward shift of the C 1s peak position is commonly observed in a-CN_x deposited by various techniques.^{6,35,53,54} The difference of XPS C 1s core level shifts between the nitrogen-doped graphene and the a-CN_x can be explained by considering whether the constitutional nitrogen atoms act as localized or delocalized electronic states in relation to the structural difference between the 2D crystal phase and 3D amorphous phase. For N-doped graphene, the localized states are formed near the nitrogen dopants in graphene, which induces a newly allowed energy state in the conduction band, and the introduction of nitrogen atoms within the graphene sub-lattice could significantly alter its local electronic and chemical properties.^{36–38} Recently, it has been experimentally and theoretically revealed that nitrogen-doped graphite has distinct localized π states in occupied and unoccupied regions near the E_F , which are derived from pyridinic-N and graphitic-N species, respectively.⁵⁵

In view of this discussion, the nitrogen atom with an ideal 2D N-doped graphene structure acts as a distinct localized electronic state, and the charge density above the N site is distributed in a local environment. In the case of 3D a-CN_x, meanwhile, the nitrogen atom could participate in delocalized interaction in addition to a localized interaction with the surrounding carbon atoms, which can be compared to a 2D graphene-like structure. It is expected that the N atoms in a 3D

a-CN_x would attract electrons from surrounding carbon atoms with the individual dipole moment, and that the negative charge density on the N sites could be distributed three-dimensionally in the bulk large area. Consequently, it contributes to a shift of the C 1s core-level line towards the higher BE side. Indeed, a nitrogen concentration of below $x = 0.04$ seems insufficient to affect the electronic state of whole C–C bonds. However, if one assumes that the a-CN_x in our system is composed of a 3D disordered network connected with some homogeneous N-doped C clusters, the individual carbon atoms should not be too far away from the nitrogen atom. In such a case, the nitrogen atom has the potential to affect the charge distribution of most of the C–C bonds, which could be a good comparison with the ideal N-doped 2D graphene. In the disordered a-CN_x structure, having both an extension and an angle distortion of the C–C bonds will induce a complex negative charge-density distribution on nitrogen. The first nearest neighbor C atoms coordinated to the nitrogen atom in a-CN_x (i.e., a localized environment) are responsible for the increase of the C 1s FWHM. In addition, some small unresolved chemical shifts originating from weakly positive charges on, for example, the second and third nearest neighbor C atoms will give rise to a broadening of the C 1s core-level line.

The N 1s spectra in Fig. 2 clearly indicate that at least two types of C–N phase (398.5 eV and 401.4 eV) exist. In terms of polarizability, the low and high BE sides are hereafter denoted as N ^{δ^-} and N ^{$\delta\delta^-$} . Here δ represents a partial charge and the negative charge strength of δ^- is stronger than $\delta\delta^-$. These two C–N components must also be included in the C 1s spectra, but the corresponding peaks are not clearly observed in the spectra because of the overlapping BE positions of these species. The difference spectra can then give us useful information to clarify the presence of significant species following the deconvolution of the multi-component spectra. Fig. 4 (left) shows the C 1s difference spectra, obtained by subtracting a-C from a-CN_x ($x = 0.027$,

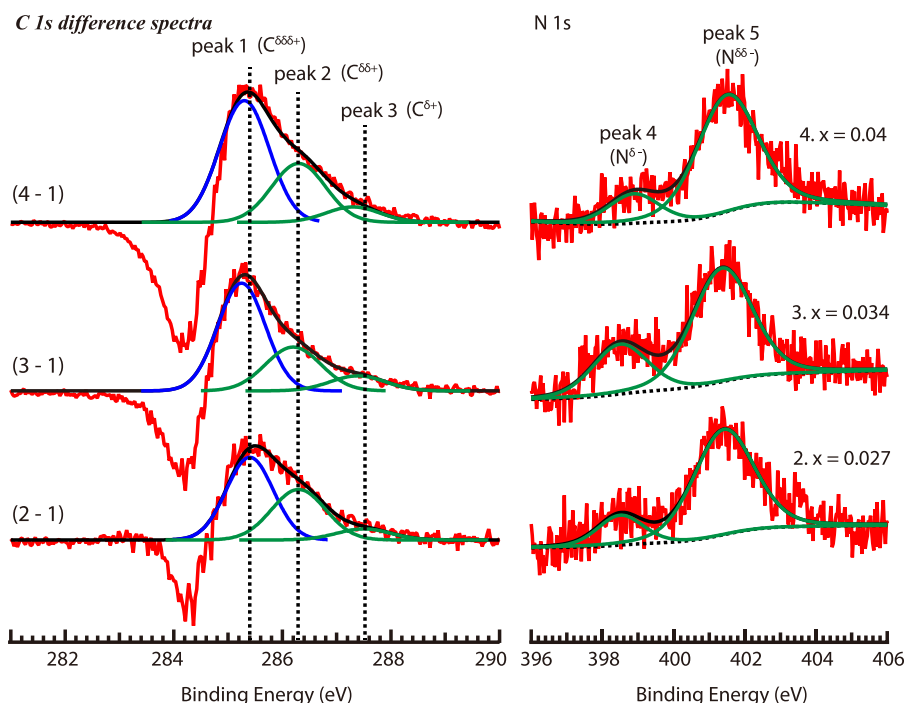


FIG. 4. (a) C 1s difference spectra based on nitrogen content x ($x = 0.027$, 0.034 , and 0.04) obtained by subtracting non-doped a-C from a-CN_x. The C 1s difference spectra have been deconvoluted with a Gaussian function. (b) The deconvoluted N 1s spectra with a Shirley-type background. Peaks 1, 2, 3, 4, and 5 are denoted as C ^{$\delta\delta\delta+$} , C ^{$\delta\delta+$} , C ^{$\delta+$} , N ^{δ^-} , and N ^{$\delta\delta^-$} , respectively.

0.034, and 0.04) and normalizing the peak intensity. The C 1s difference spectra could make clear at least three components at ~ 287.4 eV (FWHM: ~ 1.1 eV), ~ 286.3 eV (FWHM: ~ 1.2 eV), and ~ 285.4 eV (FWHM: ~ 1.2 eV), which are denoted as $C^{\delta+}$, $C^{\delta\delta+}$, and $C^{\delta\delta\delta+}$. Here the positive charge strength is in the following order, $C^{\delta+} > C^{\delta\delta+} > C^{\delta\delta\delta+}$. These three components have been deconvoluted with Gaussian fittings. The difference spectra in Fig. 4 (left) were deconvoluted with FWHM of 1.1–1.2 eV and BE difference of 0.9–1.1 eV, which will be meaningful by considering energy resolution of our XPS (Al $K\alpha$: ~ 0.85 eV). The intensity ratios of $C^{\delta+}/C^{\delta\delta+}$ for a-CN_{0.027}, a-CN_{0.034}, and a-CN_{0.04} were 0.22, 0.34, and 0.26, while the $N^{\delta-}/N^{\delta\delta-}$ ratios were 0.22, 0.41, and 0.21, respectively. A good relation was obtained between $C^{\delta+}/C^{\delta\delta+}$ and $N^{\delta-}/N^{\delta\delta-}$ ratios. Therefore, the difference spectra of Fig. 4 (left) can be used to fit the raw C 1s spectra in Fig. 5. According to the size calculation using the integrated intensity ratio of D- to G-peak in Raman spectroscopy,⁵⁶ it can be assumed that the incorporated nitrogen atoms should be apparently distributed in a carbon cluster with a size of a few nm diameter. Then the carbon atoms in such a cluster should be composed of at least fourth or fifth nearest neighbor carbons even at nitrogen content $x = 0.01$. The nitrogen atom can contribute the electronic effect to carbon atoms in the order, first, second, and third nearest neighbor carbon atoms such as N–C*, N–C–C*, and N–C–C–C*. When the carbon network is homogeneous, these species could be discriminated. If the cluster network is heterogeneous, the positive charge distribution detected in

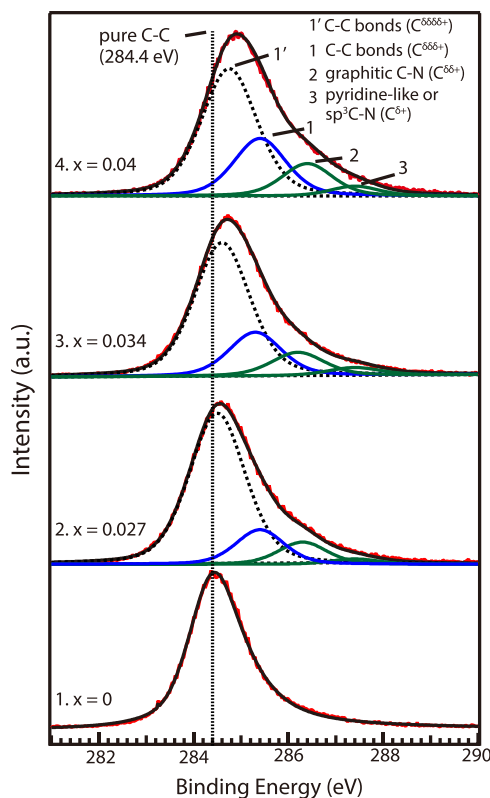


FIG. 5. The deconvoluted C 1s spectra of a-CN_x ($x = 0, 0.027, 0.034,$ and 0.04), with subtracted Shirley-type background. The dashed line shows the peak position of pure C–C bonds.

C 1s may depend on the number of carbon atoms bonded to a nitrogen atom, for instance as an average charge in alkyl groups such as methyl, ethyl, and propyl group. We are discussing the charge separation of C 1s from the viewpoint of the former homogeneous carbon network model because our carbon films were prepared under thermal equilibrium. The difference of bond character between nitrogen atom and C_n ($n = 1, 2, 3$) species is responsible for the charge separation detected in N 1s spectra. The carbon atoms have mainly the sp² character so that we can assume C=N bond formation. In such a system, two types of bonds between carbon and nitrogen atoms, such as (C_n)₃–N and (C_n)–N=C, can be imagined. Then, N 1s BE should have two different discriminated values. This will be responsible for the result that two N 1s BE values are detected to be almost constant. In general, XPS BE shift due to chemical shift is reflected for example, by electronic state, oxidation state, bonding state such as sp²/sp³, and coordination state.⁵⁷ The nitrogen substitution at the order of a few ppm into diamond leads to E_F shift and C 1s core-level shift simultaneously.⁵⁸ Heteroatom doping to high resistive materials such as intrinsic semiconductors causes increase of conductivity and E_F shift. This will be so-called charge transfer doping. In fact, it is reported that the nitrogen atoms in tetrahedral amorphous carbon is effective as an n-type dopant to shift E_F .^{8,12,59} However, our a-C films have high electrical conductivities due to sp²C-dominant amorphous structure.⁴¹ Therefore, it is considered that nitrogen incorporation to our a-C will not be so effective (or have no effect) as doping to increase the electrical conductivity and as a result no E_F shift can be detected. Consequently, the BE shift detected for C 1s in our a-C can be explained by an average charge transfer between doped nitrogen atom and surrounding carbon atoms in a-C, since XPS detects the sum up information of each electronic state on carbon atoms. The nitrogen substitution into graphene can tune the electronic band structure such as Dirac energy shift, which will be related to charge transfer between nitrogen and carbon atoms.^{38,60,61} On the other hand, the substitutional nitrogen atoms in our a-C could not be effective as an n-type dopant in contrast to the conventional charge transfer doping. In conclusion, the charge transfer in our system can be responsible for a chemical shift rather than E_F shift.

The deconvoluted N 1s spectra with a Shirley-type background of a-CN_x sample are also shown in Fig. 4 (right). Considering the electronic polarization of the C–N bond ($C^{\delta+} - N^{\delta-}$), the component labelled $N^{\delta-}$ will make the chemical bond with $C^{\delta+}$, while the peak labelled $N^{\delta\delta-}$ will do so with $C^{\delta\delta+}$. These two pairs between the C and N components can be assigned to carbon and nitrogen atoms in a-CN_x, for instance, the first and second nearest neighbor relation, whereas the C 1s component ($C^{\delta\delta\delta+}$) located at 285.4 eV does not accompany any corresponding N 1s spectra component. It is possible that the C 1s component with the BE value will be assigned to the bulk C species, which are charge transferred with only to a small extent from N atoms; i.e., the C 1s component as third and fourth nearest neighbor to N atoms, and so on. The negative component in Fig. 4 induces the substitution of the homo-polar C–C bonds at 284.4 eV in non-doped a-C for the hetero-polar C–N bonds in a-CN_x. The

negative and positive parts have to show the same spectral area in the best subtraction. At that time the spectral area should be the same at the corresponding two spectra. Note here that the relative intensity ratios ($[C^{\delta+}]/[C^{\delta\delta+}]$) are almost the same as those of $[N^{\delta-}]/[N^{\delta\delta-}]$. The numerical studies regarding N 1s core-level BE values revealed that a component with a peak at lower BE values is assigned to N atoms with isolated lone pairs in analogy with β -Si₃N₄,^{28,45} while a component with a peak at higher BE values is attributed to substitutional N atoms in a sp² graphite-like configuration. The lone pair electron in the graphite-like configuration is not isolated, and is involved in the stronger π bonds of the aromatic ring.⁴⁵ Assuming that a lone pair in pure pyridine or sp³C–N is isolated and in a local environment, the graphite-like N atom is responsible for donating a positive charge on most C–C bonds. The FWHM of the N 1s component observed in nitrogen-doped graphene is quite narrow (~ 0.8 eV).⁵² The broadening of N 1s (FWHM: ~ 2.0 eV) detected in our work infers that the negative charge density on a nitrogen atom is delocalized to affect some carbon atoms. Furthermore, the charge density distribution on each nitrogen atom will depend on the surrounding carbon network configurations to be slightly different. This is the reason for the broadening of the N 1s spectra. The large separation of ~ 3.0 eV between the lower energy (398.5 eV) and higher BE component (401.4 eV) indicates at a glance the presence of two kinds of C–N configuration with quite different electric states. The curve fittings were performed for the original spectra by considering C 1s difference spectra, as shown in Fig. 5. The data obtained in the deconvoluted C 1s and N 1s spectra are summarized Table I. The deconvoluted species 1, (denoted as C ^{$\delta\delta\delta+$}) with the peak at 285.4 ± 0.1 eV, is assigned to the weakly charge transferred C_{bulk} component affected by the nitrogen atom. Meanwhile, the deconvoluted species 1' located within a range from 284.5 to 284.8 eV is assigned to C ^{$\delta\delta\delta\delta+$} , which is the C_{bulk} component almost unaffected by nitrogen atoms. The deconvoluted species 2 (denoted as C ^{$\delta\delta+$}) that peaked at 286.3 ± 0.1 eV and the species 3 (denoted as C ^{$\delta+$}) that peaked at 287.4 eV are assigned to C 1s of a graphite-like C–N, and pyridine-like or sp³C–N, respectively. The intensity ratio of C ^{$\delta\delta\delta\delta+$} to C ^{$\delta\delta\delta+$} increased with the increase of nitrogen content in a-CN_x. This result implies that C ^{$\delta\delta\delta\delta+$} can be converted to C ^{$\delta\delta\delta+$} by the effect of nitrogen atoms.

TABLE I. Binding energy (eV), FWHM (eV), relative intensity ratio (%), and intensity ratio (C ^{$\delta+$} /C ^{$\delta\delta+$} and N ^{$\delta-$} /N ^{$\delta\delta-$}) obtained by the deconvolution of C 1s and N 1s for a-CN_{0.027}, a-CN_{0.034}, and a-CN_{0.04}.

	a-CN _{0.027}	a-CN _{0.034}	a-CN _{0.04}
C 1s	C ^{$\delta+$} , C ^{$\delta\delta+$} , C ^{$\delta\delta\delta+$} , C ^{$\delta\delta\delta\delta+$}	C ^{$\delta+$} , C ^{$\delta\delta+$} , C ^{$\delta\delta\delta+$} , C ^{$\delta\delta\delta\delta+$}	C ^{$\delta+$} , C ^{$\delta\delta+$} , C ^{$\delta\delta\delta+$} , C ^{$\delta\delta\delta\delta+$}
BE (eV)	287.4, 286.3, 285.4, 284.5	287.4, 286.2, 285.3, 284.6	287.4, 286.4, 285.4, 284.8
FWHM (eV)	1.20, 1.20, 1.20, 1.40	1.30, 1.30, 1.30, 1.38	1.20, 1.25, 1.30, 1.38
Relative intensity ratio (%)	2.2, 9.3, 14.5, 74.0	3.6, 10.8, 20.2, 65.4	3.9, 13.6, 24.7, 57.8
N 1s	N ^{$\delta-$} , N ^{$\delta\delta-$}	N ^{$\delta-$} , N ^{$\delta\delta-$}	N ^{$\delta-$} , N ^{$\delta\delta-$}
BE (eV)	398.5, 401.4	398.5, 401.4	398.8, 401.5
FWHM (eV)	1.52, 2.00	2.00, 1.83	1.67, 2.00
Relative intensity ratio (%)	17.8, 82.2	28.7, 71.3	17.4, 82.6
C ^{$\delta+$} /C ^{$\delta\delta+$}	0.24	0.33	0.29
N ^{$\delta-$} /N ^{$\delta\delta-$}	0.22	0.41	0.21

Fig. 5 requires further discussion. The presence of nitrogen atoms strongly affected the shape of the higher BE side, while it was confirmed that the tailing shape at the lower BE region below 284.4 eV was slightly changed. The tailing changes at the lower BE side originated from C–H bonds.³⁵ However, we can exclude that possibility here, since the hydrogen contents in our a-CN_x samples were almost negligible. We interpret the reason for the tailing at lower BE side here as a change in the contribution of the Gaussian and Laurentian functions induced by nitrogen incorporation. This implies that whole C–C bonds are influenced by nitrogen atoms. The increase of a Laurentian contribution by N-doping was confirmed by analyzing the fitting function.

A large number of the XPS studies on a-CN_x have focused on the local structure of the C–N bond and the origin of the two separated peaks of the N 1s core-level.^{28,45} In the present study, we discussed in detail the effects of nitrogen incorporation into a-C films on C 1s as well as N 1s core levels. Based on the C 1s difference spectra and N 1s deconvoluted spectra, we were successfully able to assign the correlated C 1s and N 1s signals to the corresponding components of a-CN_x. Recently, the effects of substitution of carbon atoms with nitrogen on the carbon bond structure have been studied by STM/STS systems and angle-resolved photoemission spectroscopy (ARPES).⁶⁰ Such recent advanced instrument will give us more insight in the present system.

C. UPS valence-band spectra

Valence-band spectra were acquired with He I excitation to investigate the effect of nitrogen incorporation on the electronic structure. The photoionization cross-section values of C 2s, C 2p, and N 2p with He I ($h\nu = 21.2$ eV) have been reported to be 1.2, 6.1, and 9.7 Mb, and 1.2, 1.9, and 4.4 Mb at He II ($h\nu = 40.8$ eV), respectively.⁶² According to the photoionization cross sections of carbon, C 2p states are dominant in He I spectra, so that they will be the main constituent of the p-derived partial density of state (p-DOS). The raw He I spectra of a-CN_x ($x = 0, 0.027, 0.034, \text{ and } 0.04$) and highly oriented pyrolytic graphite (HOPG) are shown in Fig. 6 (left). The spectra were specific in BE regions of 0–4 eV and 6–8 eV, which can be assigned to C 2p π and C 2p σ , respectively.⁶³ They were clearly

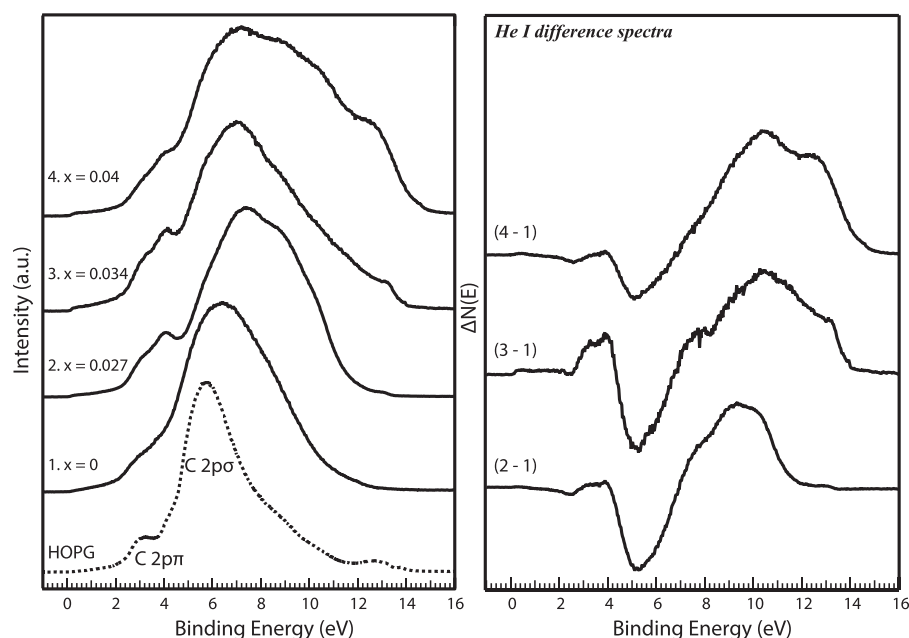


FIG. 6. He I spectra (left) with nitrogen content x ($x = 0, 0.027, 0.034,$ and 0.04). HOPG UPS spectra are shown at the bottom. The difference UPS spectra were obtained by subtracting of non-doped a-C from a-CN $_x$ (right).

discriminated as two peaks at ~ 3 and ~ 6 eV in HOPG UPS spectrum.

Compared with HOPG, the each UPS spectrum of a-CN $_x$ samples showed a broadening. This would be because they are composed of some amorphous networks. The p-DOS of a-CN $_x$ was broader than that of non-doped a-C, due to the fact that the electronic state of mother C-C bonds can be modified by nitrogen incorporation. The BE value of the peak position of C 2p σ shifted from approximately 6.5 to 7.0 eV. Nitrogen atoms in a-CN $_x$ provide more complicated p-DOS than non-doped a-C, since both C-N π bonds (C-N 2p π) and C-N σ bonds (C-N 2p σ) are included in p-DOS.⁴⁵ Thus, the interpretation for the upward shift of C 2p σ must be treated carefully.

According to the previous UPS studies on CN $_x$, assignments of the peaked components are as follows: (i) ~ 0 –3 eV to C-C 2p π ; (ii) ~ 4.5 eV to an N localized lone pair; (iii) ~ 6 eV to a C 2p π + C 2p σ overlap; (iv) ~ 6 –7 eV to a delocalized C-N 2p π ; (v) ~ 7 eV to a C-C 2p σ ; (vi) ~ 9 eV to a C-N 2p σ ; (vii) ~ 10 –11 eV to a C 2s–2p hybridized state.^{44,45,53,64} Two minor shoulders at 5–7 eV and 8–9 eV found only in a-CN $_x$ correspond to the C-N 2p π and C-N 2p σ state, respectively. Since the photoionization cross-section ratio of $\sigma(\text{N } 2p)/\sigma(\text{C } 2p)$ is 1.6 at He I excitation energy, the contribution of C-N 2p σ and 2p π states to UPS spectra will be dominant. As the C-N 2p π , C-C 2p σ and C-N 2p σ species were detected at a BE value within the range of 6–9 eV, they are difficult to distinguish from each other. In addition, C 2p σ might shift to the upper BE side with the formation of C-N bonds.

The effect of a charge-transfer between carbon and nitrogen is deduced as mentioned above. It is uncertain how such charge-transfers influence the density of states for pure C 2p σ and π bands. The peaks were clearly detected at about 4 eV, as shown in Fig. 6 (left). The peaks at ~ 4 eV in a-CN $_x$ have generally been designated as nonbonding N 2p π lone pair states analogous to those of β -Si $_3$ N $_4$; however, this has

not yet been proved for a-CN $_x$ experimentally.¹² The non-bonding N 2p $_z$ state is only possible for N atoms in a planar configuration.⁶⁵ However, it is difficult to prove whether or not N atoms are situated in the planar configuration in amorphous CN $_x$. It is not possible to completely avoid the effect of residual water (H $_2$ O) contaminating the sample surface, even under ultra-high vacuum. Irrespective of non-doped a-C and a-CN $_x$, the peak at 4 eV usually emerged after our sample had been maintained in a UHV chamber for a few hours. Consequently, the 4 eV peak will not be N lone pairs, but rather the effect of surface contamination by H $_2$ O. The effect of surface contamination should be negligible on the electronic structure of a-CN $_x$. In a-CN $_x$, the broadening of the band lying around 10–12 eV will imply a change from the C 2s–2p hybridized state to the C–N one. It is noted that the broad shoulder around 12–14 eV is associated with the secondary electron (SE) peak.

To provide insight on the interpretation of these overlapped peaks, the difference spectra were acquired by normalizing the peak intensity. Fig. 6 (right) shows the difference spectra, obtained by subtracting a-C from a-CN $_x$ ($x = 0.027, 0.034,$ and 0.04). The BE region between 0 and 3 eV due to C 2p π remained constant. The difference spectra showed the negative and positive components at 4–7 eV and 7–12 eV, respectively. The former was assigned to the upward shift of the σ band of non-doped a-C, while the latter was attributed to the contribution of C 2p π + C 2p σ overlapping to form C–N components. The delocalized C–N 2p π and C–N 2p σ were detected at BE values higher than 6 eV, so that the positive component in Fig. 6 (right) strongly infers the contribution of C–N components. This contribution can be deconvoluted by two components, the shoulder at around 7 eV and the intense component at 8–10 eV, which can be assigned to the delocalized C–N 2p π and C–N 2p σ , respectively. It has been reported that the DOS of C 2p π increases monotonously without revealing any significant nitrogen-related features as a function of nitrogen

concentration.^{35,54} However, when nitrogen concentration is enhanced considerably, the characteristic density of C–N state is dominant in the UPS spectra.^{45,53} In contrast to these findings, our results indicated that even a few nitrogen atoms could modify the valence-band structure of the a-C to the corresponding specific nitrogen-related feature. If nitrogen atoms are incorporated into distributed C clusters, they can contribute to UPS spectra much more sensitively, because of the shallow escape depth. In such a case, the DOS should reveal the contribution of C–N bonds even with low nitrogen content.

The Fermi edges of a-CN_x samples were carefully studied. The valence band spectra below the E_F were extended, as shown in Fig. 7. The Fermi edge was detected at 0 eV, not only for the non-doped a-C but also for a-CN_x samples. In addition, we could not confirm whether the Fermi level shifts or not, because of the localized state induced by nitrogen incorporation. Therefore, we cannot conclude the possibility of E_F shift from the UPS results. This result indicates that the E_F does not shift by nitrogen incorporation. Interestingly, the UPS spectra for a-CN_x exhibit some localized DOSs below the E_F . It was confirmed that nitrogen doping gives rise to at least two density states (denoted as D1 and D2), and that the D2 peak becomes significant upon nitrogen content. The origin of the DOSs below the Fermi energy by nitrogen doping has not been proved experimentally thus far. The appearance of a new DOS near the E_F for a-C:H can be made clear experimentally by photoelectron and photoelectron yield spectroscopies.⁶⁶ Two kinds of DOS have been reported at around 0.4 and 1.5 eV. It has been said that the defect state due to Si dangling bonds arises strictly from σ bond (sp³-like), whereas amorphous carbon contains both σ and π bondings.³⁹ These bonding characteristics of carbon infer that there is in principle a possibility of π (sp²-like) and σ (sp³-like) defects. It can be assumed that the defect bands are responsible for the two localized states in a-CN_x, and that they originate from both sp²-like and sp³-like defects induced by nitrogen atoms. Since nitrogen is related to the creation of a defect state, it is expected that nitrogen atoms would be captured into the carbon surrounding defects or its

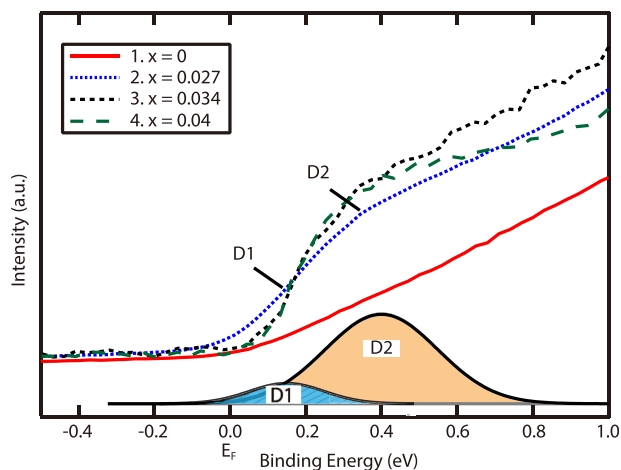


FIG. 7. UPS Fermi edge with nitrogen content x ($x=0, 0.027, 0.034,$ and 0.04). The observed two localized states are denoted as D1 and D2, and are attributed to defect bands.

defect site. In the case of N-doped graphene, the carbon atom near a defect prefers substitution by nitrogen atoms.^{67–69} The DOSs originating from the defects could be clearly observed by UPS spectra after a-CN_x samples were exposed to air for a long time. This indicates that the defect sites can be stabilized by nitrogen atoms; that is, that nitrogen atom can contribute to chemical stability on the surface. It is reported that N-doping onto the graphene lattices decreases the surface oxygen-containing groups, which may improve the corrosion resistance of the graphene.⁷⁰ The chemical stability gained by nitrogen doping is discussed further below.

Recently, the effect of N doping on the formation of structural defects has been intensively studied in compounds such as N-doped graphene, the NV center in diamond, and graphitic C₃N₄ (g-C₃N₄).^{25,71,72} We believe that our UPS results provide an insight into the relationship between nitrogen incorporation into a-C and the creation of defects.

D. Photoelectron spectroscopy (XPS/UPS) studies on adsorption and reactions with NO probe molecules

Fig. 8 shows O 1s spectra for a series of heating and NO exposures, and the difference spectra between two successive experiments. Before NO exposure, the O 1s signal was detected at 3.1 at.%. The O 1s spectrum was broad and asymmetric, and could be deconvoluted into three components at 531 eV (O²⁻), 532.5 eV (–OH species), and 534 eV (residual carbonate species CO_x).^{73–75} Upon exposure to NO gas (3600 L) at r.t., an additional component was observed at ~532 eV. The oxygen content increased slightly from 3.1 at. % to 3.6 at. %. In contrast to O 1s, the N 1s spectrum had no signal. The O 1s BE values for several adsorbed NO_x species have been identified as follows: (i) ~531–532 eV to adsorbed NO molecular; (ii) ~532–533 eV to adsorbed NO₂; (iii) ~533–534.5 eV to adsorbed N₂O; and (iv) 529–531 eV to dissociatively adsorbed atomic oxygen O(a).^{75–77} Therefore, we can assign the component at ~532 eV to the adsorbed NO species. The broad peak could indicate the presence of different kinds of adsorbed NO states and/or partially dissociated NO species.

It is widely known that some defects play a crucial role in molecular-gas-adsorption on materials such as metals, metal oxides, and carbon nanotube.^{78–80} Since a-C will have some defects with higher density because of its disordered structure, it is reasonable to assume that they will act as NO adsorption sites. After heating the sample at 873 K for 4 h, the oxygen content decreased from 3.5 at. % to 3.1 at. %. The O 1s spectrum was completely changed, and the intensity of the O²⁻ component at ~531 eV was dramatically increased. The difference spectrum in Fig. 8(c – b) shows the increase of the component at 531 eV and its decrease at 533 eV, implying that some oxygen species (–OH, CO_x) are replaced by the reaction with NO(a) to form O²⁻ species. Since NO molecules can be dissociatively adsorbed on some metal surfaces,⁴⁰ the dissociated O(a) may arise from the dissociation of NO molecules on the a-C surface. We were not able to confirm the dissociation of NO molecules, because the corresponding N 1s signal could not be detected.

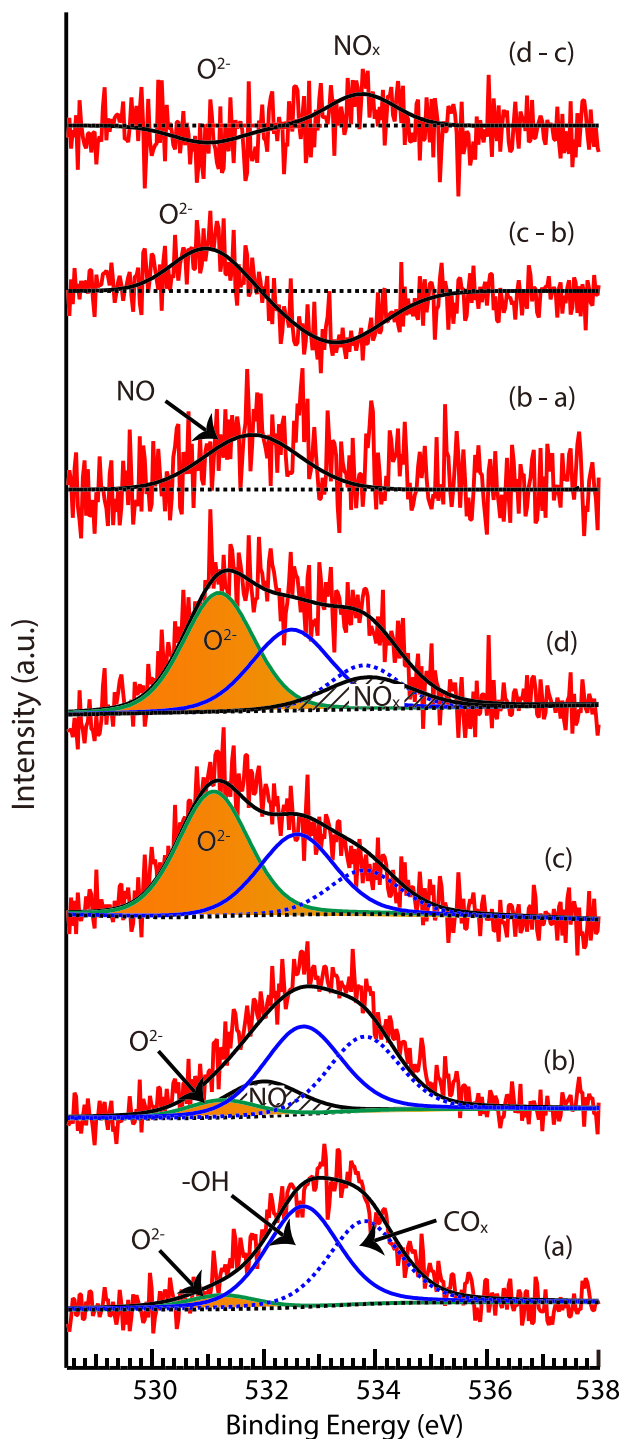


FIG. 8. XPS O 1s spectra and difference spectra of a-C for a series of heating and NO exposures: (a) before NO exposure; (b) after first NO exposure (3600L) at r.t.; (c) after heating at 873 K; and (d) after second NO exposure (3600L) at r.t.

Fig. 8(d) shows the O 1s spectrum at the second NO exposure (3600L) after heating at 873 K. The oxygen content increased from 3.1 at.% to 3.3 at.% with a slight increase of relative intensity at ~ 534.2 eV. The O 1s spectrum peak at ~ 534.2 eV can be attributed to NO_x (NO_2 , NO_3 , and N_2O), including NO species that interacted with O atoms (NO-O).^{81–83} The effects of surface oxygen on NO adsorption and reaction have been extensively studied on several metals, which found that the NO-O intermediate

states were initially formed in a coadsorption experiment of NO and O_2 molecules on clean Pt and Ag surfaces. The strong NO-O interaction leads to the formation of NO_x species simultaneously with the dissociation of $\text{O(a)} + \text{N(a)}$.^{82,83} In our results, the appearance of a new component at ~ 534.2 eV with the decrease of O^{2-} component indicates that adsorbed NO_x are formed via a concerted mechanism between NO(a) and O(a).

Fig. 9 shows the O 1s spectra before and after NO exposure on a- $\text{CN}_{0.03}$ and the difference spectrum. After NO exposure (3600L), the oxygen content increased from 2.2 at.% to 3.2 at.%. The component at ~ 534.3 eV, which is attributed to both NO_x and NO-O species, increased, while the intensity of O^{2-} species at ~ 531.2 eV slightly decreased. The interaction of NO(a) with O^{2-} will occur for a- CN_x as well as a-C samples. When the O^{2-} species on the surface react with NO (molecular), the negative area at ~ 531.2 eV should be almost the same, with a positive area at ~ 534.3 eV. As shown in the difference spectrum of Fig. 9, the area difference between the positive and negative regions indicates that a portion of the adsorbed NO species was dissociative and adsorbed to oxygen atoms via the NO-O interaction; consequently, the dissociative oxygen atoms are used to form NO_x (a).

In NO exposure experiments for a-C, we observed the component at ~ 532 eV associated with NO(a) on defect sites, whereas this was not the case for a- $\text{CN}_{0.03}$. It was expected that a-C should have defect sites at a much higher concentration than a- $\text{CN}_{0.03}$. As already mentioned for the

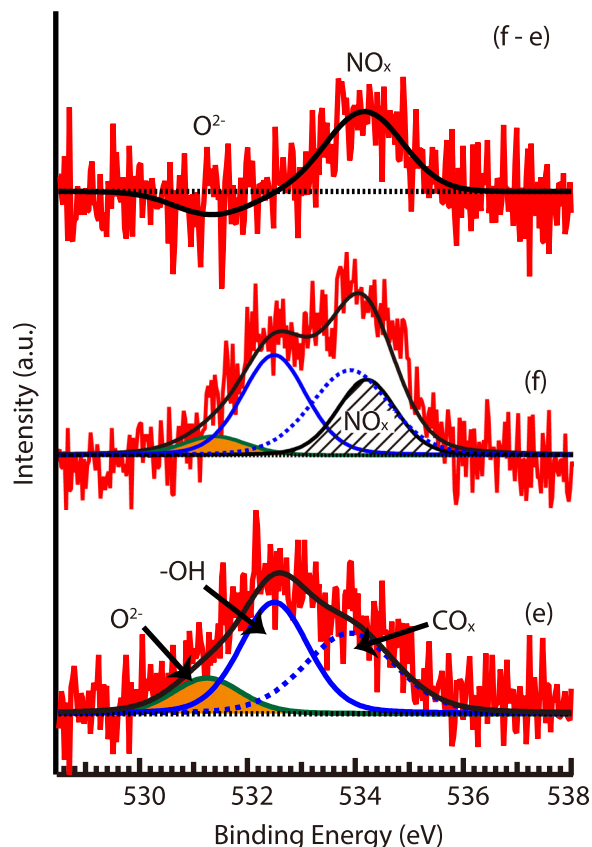


FIG. 9. XPS O 1s spectra and difference spectrum of a- $\text{CN}_{0.03}$ for before and after NO exposure: (a) before NO exposure and (b) after NO exposure (3600L) at r.t.

UPS spectra of a-CN_x, the incorporation of nitrogen atoms into a-C is related to the creation of steady defect sites, and NO molecules are not adsorbed molecularly on the defect sites of a-CN_x. In addition, oxygen content on a-CN_x before NO exposure was lower than that on a-C. This result indicates that the number of surface defects especially active for NO dissociation is reduced by terminated nitrogen atoms, and as a result, a-CN_x will have lower activity for NO adsorption. In the case of NO adsorption on O²⁻ species at ~531 eV, we observed the presence of a NO_x-related component at ~534 eV for both a-C and a-CN_{0.03}. This indicates that O²⁻ species can act as a NO adsorption site independent of nitrogen incorporation.

Interestingly, the C 1s main peak of a-C showed an upward shift to the higher BE side from 284.4 to 284.6 eV after NO exposure, while there was no such shift for a-CN_{0.03}. In the second NO exposure experiment, after heating at 873 K, the C 1s of a-C shifted toward the higher BE side from 284.2 to 284.5 eV. Such a BE shift after NO adsorption on a-C will induce an electron transfer from NO(a) to the surface. We earlier concluded that even a few atom percentage points of nitrogen atoms lead to a shift of C 1s toward the higher BE side by the charge transfer from C to N. Similarity, the shift to the higher BE side after NO exposure indicates that even a small amount of adsorbed NO can donate a positive charge on some surface carbon atoms. Then, the adsorbed NO and NO_x species should have negative charges, which are denoted as NO⁻ and NO_x⁻, respectively. For a-CN_x, since most carbon on the surface already has a positive charge from the incorporated nitrogen atoms, the C 1s BE value will be unaffected by adsorbed NO_x species.

The UPS spectra before and after NO exposure on a-C and the difference spectrum are shown in Fig. 10. The difference spectrum (b - a) makes clear the additional peaks at ~3.5, ~4.2, ~6.5, ~8.8, ~11, and ~13 eV below the E_F. The peaks located at ~3.5, ~8.8, ~11, and ~14 eV can be assigned to 2π, 1π, 5σ, and 4σ, respectively, which are derived from the valence orbitals of the adsorbed NO molecule.⁸⁴ The broad peaks located at ~4.2 and ~6.5 eV can be attributed to the atomic orbitals of N and O 2p levels, respectively.^{76,85,86} The presence of N and O atoms could not be clearly observed in the XPS spectrum because of the large escape depth, i.e., the less sensitive surface. Note that the dissociative N and O atoms coexist with the adsorbed NO species on the surface.

The difference spectrum (d - c) at the second NO exposure after heating the sample at 873 K was similar to that of the first NO exposure experiment except for the disappearance of ~3.5 and ~13 eV. Since the XPS O 1s indicates the presence of both of NO-O and NO_x species, these peaks would be detected in the UPS spectrum. The UPS spectra of molecularly adsorbed N₂O present four peaks at 5.9, 9.3, 11.0, and 12.8 eV, which are assigned as 2π, 7σ, 1π, and 6σ, respectively.^{87,88} Molecularly adsorbed NO₂ produces a complex structure with a large number of orbitals.⁸⁹ In this study, several NO_x species were found to coexist with concerted NO-O species in addition to dissociative N and O atoms on the surface due to the large amount of NO (3600 L) dosed at r.t. The additional peaks that appeared after the second NO exposure can be primarily assigned as a part of the

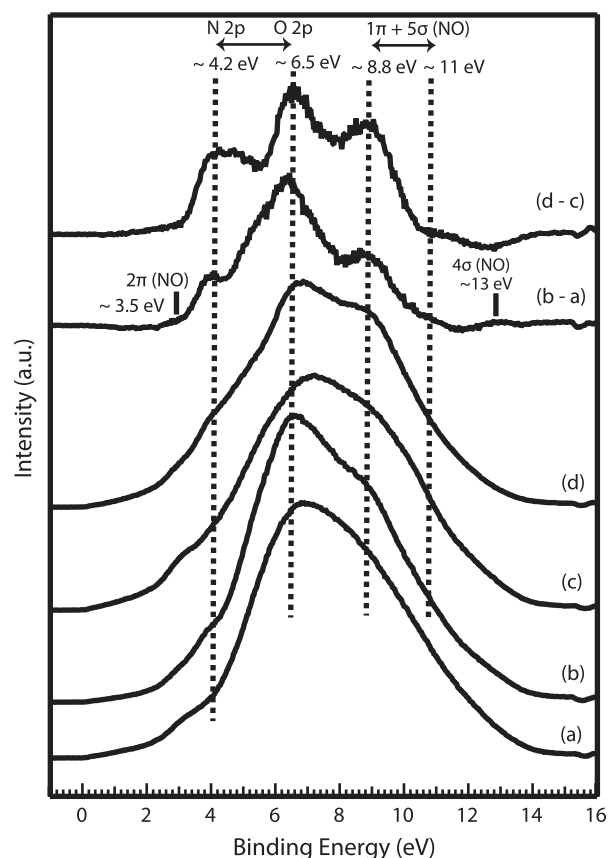


FIG. 10. UPS spectra and difference spectra of a-C for a series of heating and NO exposures: (a) before NO exposure; (b) after first NO exposure (3600 L) at r.t.; (c) after heating at 873 K; (d) after second NO exposure (3600 L) at r.t.

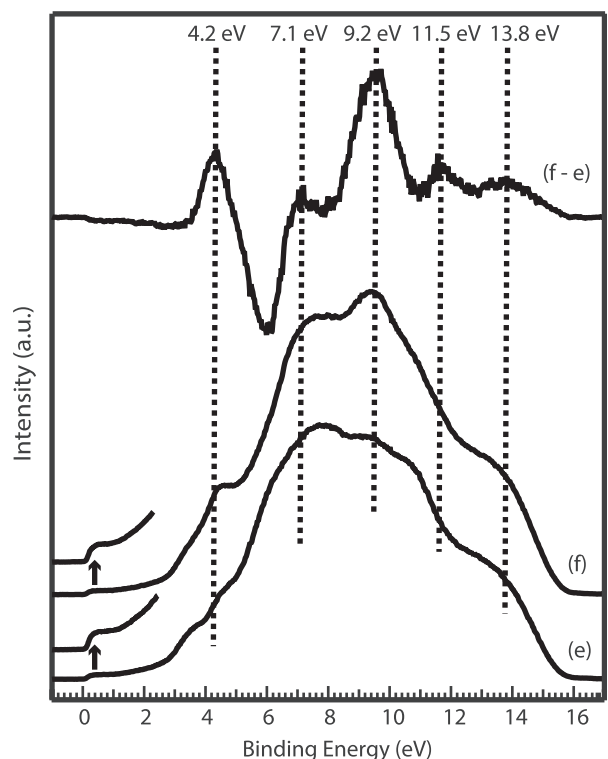


FIG. 11. UPS spectra and difference spectrum of a-CN_{0.03} before and after NO exposure: (a) before NO exposure and (b) after NO exposure (3600 L) at r.t.

TABLE II. Summarized data obtained in NO adsorption and reaction experiments by XPS/UPS measurements.

Sample	Atomic ratio C:O:N	XPS		UPS
		O 1 s BE (eV)	C 1 s BE (eV)	Difference spectra BE (eV)
a-C				
(a) Before	100:3.2:0	~531, ~532.5, ~534	284.4	(b – a)
(b) NO 3600 L	100:3.8:0	~531, ~532 ^a , ~532.5, ~534	284.6	~3.5, ~4.2, ~6.5, ~8.8, ~11, ~13
(c) 873 K	100:3.2:0	~531, ~532.5, ~534	284.2	(d – c)
(d) NO 3600 L	100:3.4:0	~531, ~532.5, ~534, ~534.2 ^b	284.5	~4.2, ~6.5, ~8.8, ~11
a-CN _{0.03}				
(e) Before	100:2.2:3.2	~531.2, ~532.5, ~534	285.0	(f – e)
(f) NO 3600 L	100:3.2:3.3	~531.2, ~532.5, ~534, ~534.3 ^b	285.0	~4.2, ~7.1, ~9.2, ~11.5, ~13.8

^aNO species.^bNO_x species and/or NO–O species.

NO_x-associated molecular orbitals, such as adsorbed NO, N₂O, and NO₂, in addition to the concerted NO–O species.

Fig. 11 shows the UPS spectra of a-CN_{0.03} before and after NO exposure. After NO exposure at 3600 L, five components were found at ~4.2, ~7.1, ~9.2, ~11.5, and 13.8 eV. The first two components at ~4.2 and ~7.1 eV can be assigned to dissociative N and O atoms, respectively. The latter three components at ~9.2, ~11.5, and 13.8 eV, meanwhile, are in good agreement with the 1 π , 5 σ , and 4 σ of molecularly adsorbed NO orbitals with the lack of 2 π level. The XPS result after NO exposure indicates the presence of NO_x species, so that the corresponding molecular orbitals should be included in the UPS spectrum of not only a-CN_{0.03} but also a-C. The negative peak at ~6 eV can be interpreted as the emission loss of C 2p, because the a-CN_{0.03} surface can be covered by adsorbed NO_x species at a much higher concentration than the a-C. This may simultaneously explain the selective electronic interaction between NO_x species and C 2p orbitals on a-CN_{0.03} in addition to the higher photoionization cross section of C 2p (6.1 Mb) compared with C 2s (1.2 Mb). The defect states below the E_F remained almost constant even after NO exposure, which implies that the defect states created by nitrogen incorporation are quite stable, as mentioned above.

The data obtained in this work are summarized in Table II. From the XPS/UPS results, it is possible to conclude that NO adsorption and the following reactions to produce NO_x species occur on defect sites and/or O²⁻. As for a-C, both the defect sites and O²⁻ species act as NO adsorption sites. Meanwhile, for a-CN_x, O²⁻ species will be restrictively responsible for NO adsorption because incorporating nitrogen atoms decreased the number of defect sites. This is due to the fact that the a-CN_x surface is much more chemically stable than the a-C surface. Furthermore, it is noteworthy that it can be inferred that the NO adsorption occurs on both a-C and a-CN_x surfaces, which could awaken the potential application of carbon-based amorphous materials for catalytic reactions of NO_x species, as well as NO molecules.

IV. CONCLUSIONS

We investigated the effects of nitrogen incorporation on the electronic structure of a-C using photoelectron spectroscopy (XPS/UPS). In the 3D a-CN_x phase, the incorporated

nitrogen atoms induce positive charge distribution of most of the C–C bonds, and result in a slight shift of C 1s core-level toward the higher BE side. Even a few nitrogen atoms can provide a delocalized charge contribution to the surrounding carbon atoms. The C 1s difference spectra reveal that there are two different C–N bond types, and that bulk C–C components are charge transferred by N atoms incorporated to affect the second and third nearest neighbor C atoms. The C–C species with the lowest C 1s BE value are influenced (charge transferred) by nitrogen atoms and finally converted to C 1s species at 285.4 eV with an increase of nitrogen content. Even a slightly higher percentage of nitrogen can modify the DOS of a-C; however, the shift of the E_F cannot be detected by nitrogen incorporation. The N-doping produces two localized defect states below the E_F . These defect sites play significant roles in terms of surface reactivity based on the electronic nature of a-CN_x. The studies on adsorption and reactions with NO molecules make clear the presence of two kinds of local sites for NO adsorption. For a-C, both defect sites and O²⁻ species are responsible not only for NO adsorption but also for the reaction, while for a-CN_x, NO can be adsorbed on O²⁻ species. Nitrogen doping reduces the defect density of the a-C and while at the same time inducing chemical stability of the surface. The difference of the reactivity between a-C and a-CN_x originates from the chemical stability of the surface.

¹A. Grill, *Diamond Relat. Mater.* **8**, 428 (1999).²Y. Lifshitz, *Diamond Relat. Mater.* **8**, 1659 (1999).³A. Erdemir and C. Donnet, *J. Phys. D: Appl. Phys.* **39**, R311 (2006).⁴J. Vetter, *Surf. Coat. Technol.* **257**, 213 (2014).⁵J. Robertson, *Mater. Sci. Eng., R* **37**, 129 (2002).⁶C. Ronning, E. Dreher, J.-U. Thiele, P. Oelhafen, and H. Hofsäss, *Diamond Relat. Mater.* **6**, 830 (1997).⁷V. S. Veerasamy, G. A. J. Amaratunga, C. A. Davis, A. E. Timbs, W. I. Milne, and D. R. McKenzie, *J. Phys.: Condens. Matter* **5**, L169 (1993).⁸V. S. Veerasamy, J. Yuan, G. A. J. Amaratunga, W. I. Milne, K. W. R. Gilkes, M. Weiler, and L. M. Brown, *Phys. Rev. B* **48**, 17954 (1993).⁹C. Ronning, U. Griesmeier, M. Gross, H. C. Hofsäss, R. G. Downing, and G. P. Lamaze, *Diamond Relat. Mater.* **4**, 666 (1995).¹⁰S. R. P. Silva, J. Robertson, G. A. J. Amaratunga, B. Rafferty, L. M. Brown, J. Schwan, D. F. Franceschini, and G. Mariotto, *J. Appl. Phys.* **81**, 2626 (1997).¹¹J. Schwan, V. Batori, S. Ulrich, H. Ehrhardt, and S. R. P. Silva, *J. Appl. Phys.* **84**, 2071 (1998).¹²J. Robertson and C. A. Davis, *Diamond Relat. Mater.* **4**, 441 (1995).¹³T. Köhler, G. Jungnickel, and T. Frauenheim, *Phys. Rev. B* **60**, 10864 (1999).

- ¹⁴F. Alibart, O. D. Drouhin, M. Benlahsen, S. Muhl, S. E. Rodil, E. Camps, and L. Escobar-Alarcon, *Appl. Surf. Sci.* **254**, 5564 (2008).
- ¹⁵A. Y. Liu and M. L. Cohen, *Phys. Rev. B* **41**, 10727 (1990).
- ¹⁶N. Hellgren, M. P. Johansson, E. Broitman, L. Hultman, and J.-E. Sundgren, *Phys. Rev. B* **59**, 5162 (1999).
- ¹⁷W. J. Gammon, D. I. Malyarenko, O. Kraft, G. L. Hoatson, A. C. Reilly, and B. C. Holloway, *Phys. Rev. B* **66**, 153402 (2002).
- ¹⁸W. J. Gammon, G. L. Hoatson, B. C. Holloway, R. L. Vold, and A. C. Reilly, *Phys. Rev. B* **68**, 195401 (2003).
- ¹⁹T. W. Scharf, R. D. Ott, D. Yang, and J. A. Barnard, *J. Appl. Phys.* **85**, 3142 (1999).
- ²⁰S. Meskinis, R. Gudaitis, V. Kopustinskas, S. Tamulevičius, and K. Šlapikas, *Diamond Relat. Mater.* **19**, 1249 (2010).
- ²¹H. Wang, T. Maiyalagan, and X. Wang, *ACS Catal.* **2**, 781 (2012).
- ²²C. P. Ewels and M. Glerup, *J. Nanosci. Nanotechnol.* **5**, 1345 (2005).
- ²³A. Thomas, A. Fischer, F. Goettmann, M. Antonietti, J.-O. Müller, R. Schlögl, and J. M. Carlsson, *J. Mater. Chem.* **18**, 4893 (2008).
- ²⁴J. Zhu, P. Xiao, H. Li, and S. A. C. Carabineiro, *ACS Appl. Mater. Interfaces* **6**, 16449 (2014).
- ²⁵A. Gruber, A. Dräbenstedt, C. Tietz, L. Fleury, J. Wrachtrup, and C. von Borczyskowski, *Science* **276**, 2012 (1997).
- ²⁶S. Muhl and J. M. Méndez, *Diamond Relat. Mater.* **8**, 1809 (1999).
- ²⁷H. Sjöström, S. Stafström, M. Boman, and J.-E. Sundgren, *Phys. Rev. Lett.* **75**, 1336 (1995).
- ²⁸D. Marton, K. J. Boyd, A. H. Al-Bayati, S. S. Todorov, and J. W. Rabalais, *Phys. Rev. Lett.* **73**, 118 (1994).
- ²⁹Z. J. Zhang, S. Fan, and C. M. Lieber, *Appl. Phys. Lett.* **66**, 3582 (1995).
- ³⁰W.-D. Wu, J. Ni, X.-M. Wang, X.-D. Yang, Z.-M. Chen, and Y.-J. Tang, *Vacuum* **83**, 1397 (2009).
- ³¹F. Alibart, O. D. Drouhin, C. Debiemme-Chouvy, and M. Benlahsen, *Solid State Commun.* **145**, 392 (2008).
- ³²J. Q. Wu, X. C. Wang, E. Y. Jiang, and H. L. Bai, *Appl. Surf. Sci.* **255**, 9498 (2009).
- ³³Z. J. Zhang, S. Fan, J. Huang, and C. M. Lieber, *Appl. Phys. Lett.* **68**, 2639 (1996).
- ³⁴E. Broitman, N. Hellgren, K. Järrendahl, M. P. Johansson, S. Olafsson, G. Radnóczy, J.-E. Sundgren, and L. Hultman, *J. Appl. Phys.* **89**, 1184 (2001).
- ³⁵A. Mansour and D. Ugolini, *Phys. Rev. B* **47**, 10201 (1993).
- ³⁶L. Zhao, R. He, K. T. Rim, T. Schiros, K. S. Kim, H. Zhou, C. Gutiérrez, S. P. Chockalingam, C. J. Arguello, L. Pálová, D. Nordlund, M. S. Hybertsen, D. R. Reichman, T. F. Heinz, P. Kim, A. Pinczuk, G. W. Flynn, and A. N. Pasupathy, *Science* **333**, 999 (2011).
- ³⁷R. Lv, Q. Li, A. R. Botello-Méndez, T. Hayashi, B. Wang, A. Berkdemir, Q. Hao, A. L. Elías, R. Cruz-Silva, H. R. Gutiérrez, Y. A. Kim, H. Muramatsu, J. Zhu, M. Endo, H. Terrones, J.-C. Charlier, M. Pan, and M. Terrones, *Sci. Rep.* **2**, 586 (2012).
- ³⁸F. Joucken, Y. Tison, J. Lagoute, J. Dumont, D. Cabosart, B. Zheng, V. Repain, C. Chacon, Y. Girard, A. R. Botello-Méndez, S. Rousset, R. Sporcken, J.-C. Charlier, and L. Henrard, *Phys. Rev. B* **85**, 161408 (2012).
- ³⁹J. Robertson and E. P. O'Reilly, *Phys. Rev. B* **35**, 2946 (1987).
- ⁴⁰W. A. Brown and D. A. King, *J. Phys. Chem. B* **104**, 2578 (2000).
- ⁴¹Y. Murata, C.-K. Choo, H. Ono, Y. Nagai, and K. Tanaka, *Mater. Today* **3**, S197 (2016).
- ⁴²T. Iijima, C.-K. Choo, and K. Tanaka, Japan Patent No. 5002803 (1 January 2012).
- ⁴³K. Nakamura, C.-K. Choo, and K. Tanaka, Japan Patent No. 5240978 (1 April 2013).
- ⁴⁴N. Hellgren, J. Guo, Y. Luo, C. Sâthe, A. Agui, S. Kashtanov, J. Nordgren, H. Ågren, and J.-E. Sundgren, *Thin Solid Films* **471**, 19 (2005).
- ⁴⁵S. Souto, M. Pickholz, M. C. dos Santos, and F. Alvarez, *Phys. Rev. B* **57**, 2536 (1998).
- ⁴⁶S. E. Rodil and S. Muhl, *Diamond Relat. Mater.* **13**, 1521 (2004).
- ⁴⁷W. J. Gammon, O. Kraft, A. C. Reilly, and B. C. Holloway, *Carbon* **41**, 1917 (2003).
- ⁴⁸C. Ronning, H. Feldermann, R. Merk, H. Hofsäss, P. Reinke, and J.-U. Thiele, *Phys. Rev. B* **58**, 2207 (1998).
- ⁴⁹R. J. Koch, M. Weser, W. Zhao, F. Viñes, K. Gotterbarm, S. M. Kozlov, O. Höfert, M. Ostler, C. Papp, J. Gebhardt, H.-P. Steinrück, A. Görling, and Th. Seyller, *Phys. Rev. B* **86**, 075401 (2012).
- ⁵⁰Y.-C. Lin, C.-Y. Lin, and P.-W. Chiu, *Appl. Phys. Lett.* **96**, 133110 (2010).
- ⁵¹L. Pauling, *The Chemical Bond: A Brief Introduction to Modern Structural Chemistry* (Cornell University Press, New York, 1960), p. 64.
- ⁵²Z. Luo, S. Lim, Z. Tian, J. Shang, L. Lai, B. MacDonald, C. Fu, Z. Shen, T. Yu, and J. Lin, *J. Mater. Chem.* **21**, 8038 (2011).
- ⁵³P. Hammer, N. M. Victoria, and F. Alvarez, *J. Vac. Sci. Technol. A* **16**, 2941 (1998).
- ⁵⁴S. Bhattacharyya, C. Cardinaud, and G. Turban, *J. Appl. Phys.* **83**, 4491 (1998).
- ⁵⁵T. Kondo, S. Casolo, T. Suzuki, T. Shikano, M. Sakurai, Y. Harada, M. Saito, M. Oshima, M. I. Trioni, G. F. Tantardini, and J. Nakamura, *Phys. Rev. B* **86**, 035436 (2012).
- ⁵⁶A. C. Ferrari and J. Robertson, *Philos. Trans. R. Soc. London, Ser. A* **362**, 2477 (2004).
- ⁵⁷D. Briggs and M. P. Seah, *Practical Surface Analysis*, 2nd ed., Auger and X-ray Photoelectron Spectroscopy Vol. 1 (John Wiley & Sons, Chichester, 1990).
- ⁵⁸A. T. Collins, *J. Phys.: Condens. Matter* **14**, 3743 (2002).
- ⁵⁹A. A. Valladares, A. Valladares, R. M. Valladares, and M. A. McNelis, *J. Non-Cryst. Solids* **231**, 209 (1998).
- ⁶⁰F. Joucken, Y. Tison, P. L. Fèvre, A. Tejada, A. Taleb-Ibrahimi, E. Conrad, V. Repain, C. Chacon, A. Bellec, Y. Girard, S. Rousset, J. Ghijsen, R. Sporcken, H. Amara, F. Ducastelle, and J. Lagoute, *Sci. Rep.* **5**, 14564 (2015).
- ⁶¹E. Velez-Fort, C. Mathieu, E. Pallecchi, M. Pigneur, M. G. Silly, R. Belkhou, M. Marangolo, A. Shukla, F. Sirotti, and A. Ouerghi, *ACS Nano* **6**, 10893 (2012).
- ⁶²J. J. Yeh and I. Lindau, *Atomic Data Nucl. Data Tables* **32**, 1 (1985).
- ⁶³F. R. McFeely, S. P. Kowalczyk, L. Ley, R. G. Cavell, R. A. Pollak, and D. A. Shirley, *Phys. Rev. B* **9**, 5268 (1974).
- ⁶⁴A. Bianconi, S. B. M. Hagström, and R. Z. Bachrach, *Phys. Rev. B* **16**, 5543 (1977).
- ⁶⁵R. Kärcher, L. Ley, and R. L. Johnson, *Phys. Rev. B* **30**, 1896 (1984).
- ⁶⁶J. Schäfer, J. Ristein, and L. Ley, *Diamond Relat. Mater.* **3**, 861 (1994).
- ⁶⁷B. Guo, Q. Liu, E. Chen, H. Zhu, L. Fang, and J. R. Gong, *Nano Lett.* **10**, 4975 (2010).
- ⁶⁸X. Wang, X. Li, L. Zhang, Y. Yoon, P. K. Weber, H. Wang, J. Guo, and H. Dai, *Science* **324**, 768 (2009).
- ⁶⁹G. Imamura and K. Saiki, *Chem. Phys. Lett.* **587**, 56 (2013).
- ⁷⁰D. Geng, S. Yang, Y. Zhang, J. Yang, J. Liu, R. Li, T.-K. Sham, X. Sun, S. Ye, and S. Knights, *Appl. Surf. Sci.* **257**, 9193 (2011).
- ⁷¹X. Li, D. Geng, Y. Zhang, X. Meng, R. Li, and X. Sun, *Electrochem. Commun.* **13**, 822 (2011).
- ⁷²P. Niu, G. Liu, and H.-M. Cheng, *J. Phys. Chem. C* **116**, 11013 (2012).
- ⁷³D. Y. Zemlyanov, E. Savinova, A. Scheybal, K. Doblhofer, and R. Schlögl, *Surf. Sci.* **418**, 441 (1998).
- ⁷⁴T. Herranz, X. Deng, A. Cabot, Z. Liu, and M. Salmeron, *J. Catal.* **283**, 119 (2011).
- ⁷⁵T. Shimada, B. S. Mun, I. F. Nakai, A. Banno, H. Abe, Y. Iwasawa, T. Ohta, and H. Kondoh, *J. Phys. Chem. C* **114**, 17030 (2010).
- ⁷⁶C. R. Brundle, *J. Vac. Sci. Technol.* **13**, 301 (1976).
- ⁷⁷J. L. Bischoff, L. Kubler, and D. Bolmont, *Phys. Rev. B* **39**, 3653 (1989).
- ⁷⁸F. Mercuri, A. Sgamellotti, L. Valentini, I. Armentano, and J. M. Kenny, *J. Phys. Chem. B* **109**, 13175 (2005).
- ⁷⁹A. Kolmakov, J. Stultz, and D. W. Goodman, *J. Chem. Phys.* **113**, 7564 (2000).
- ⁸⁰M. W. Roberts and R. St. C. Smart, *Surf. Sci.* **100**, 590 (1980).
- ⁸¹E. Ozensoy, C. H. F. Peden, and J. Szanyi, *J. Phys. Chem. B* **109**, 15977 (2005).
- ⁸²G. Polzonetti, P. Alnot, and C. R. Brundle, *Surf. Sci.* **238**, 226 (1990).
- ⁸³R. I. Masel, E. Umbach, J. C. Fuggle, and D. Menzel, *Surf. Sci.* **79**, 26 (1979).
- ⁸⁴M. E. Bartram, B. E. Koel, and E. A. Carter, *Surf. Sci.* **219**, 467 (1989).
- ⁸⁵S. Tatarenko, M. Alnot, and R. Ducros, *Surf. Sci.* **163**, 249 (1985).
- ⁸⁶T. Kioka, *Surf. Sci.* **222**, 140 (1989).
- ⁸⁷J. Kiss, D. Lennon, S. K. Jo, and J. M. White, *J. Phys. Chem.* **95**, 8054 (1991).
- ⁸⁸E. Umbach and D. Menzel, *Chem. Phys. Lett.* **84**, 491 (1981).
- ⁸⁹C. R. Brundle, D. Neumann, W. C. Price, D. Evans, A. W. Potts, and D. G. Streets, *J. Chem. Phys.* **53**, 705 (1970).